METALURGI
Majalah Ilmu dan Teknologi
p-ISSN 0126-3188 | e-ISSN 2443-3926
ejurnalmaterialmetalurgi.lipi.go.id

CHARACTERIZATION AND ANALYSIS OF HARDNESS, MICROSTRUCTURE, AND CRYSTALLOGRAPHY OF SS 304-SHEATHED MgB_2 SUPERCONDUCTING WIRES

Rizky Ramadhani Rivai[a], Andika Widya Pramono[b*], Tri Hardi Priyanto[c], Awan Maghfirah[a]

[a]Physics Study Program, University of North Sumatra
Jl. Dr. T. Mansur No. 9, Medan, Sumatera Utara, Indonesia 20222
[b]Research Center for Advanced Materials, National Research and Innovation Agency
[c]Research Center for Radiation Detection and Nuclear Analysis Technology,
National Research and Innovation Agency
B.J. Habibie Sains and Technology Area, Banten, Indonesia 15314
*E-mail: andi010@brin.go.id

Received: 07-01-2023, Revised: 16-05-2023, Accepted: 19-05-2023

Abstract

This research was conducted to analyze the hardness, microstructural morphology, and crystallography of the MgB_2 compound in the form of a SS 304-sheathed superconducting wire. MgB_2 superconducting wire with SS 304 outer sheath was manufactured using an ex-situ rolling process. The results of the Vickers hardness test with a load of 0.3 N showed the MgB_2 hardness value of 355.1 HV. The results of observations with SEM-EDS (scanning electron microscopy-energy dispersive spectroscopy) showed the agglomerations of the second phase of (Mg)B-O with various compositions due to the rolling process. There was also a longitudinal crack in the MgB_2 area due to the work-hardening phenomenon in the brittle MgB_2 solid. There were no obvious Bragg peaks in the MgB_2 phase. The detected Bragg peaks came from the austenitic (γ-Fe) of SS 304-sheath.

Keywords: *Magnesium diboride, agglomeration, FCD/TD, crystallographic texture, neutron absorption*

1. INTRODUCTION

Superconductors are materials capable of conducting electric current with zero resistivity at very low temperatures. Superconductors can conduct current even in the absence of a voltage source. This material can also act as a perfect diamagnetic material, so it can completely reject the external magnetic field as long as it is below its critical value (Hc) [1]. Magnesium diboride (MgB_2), which was discovered in 2001 by Nagamatsu et al., [2] is a metal-based superconducting material with a critical temperature (Tc) of 39 K, so that it can be used in the operational temperature range of 20-25 K in more economical cryocooler conditions. The research and development of MgB2 are expected to replace the low-temperature superconducting materials NbTi and Nb_3Sn due to the higher Tc of MgB_2. In addition, Mg is an abundant and cheaper metal resource compared to Nb, Ti, and Sn. Superconducting applications are usually used in the form of wire or tape. In this study, the process of making wire was carried out using the ex-situ powder-in-tube method. Using the ex-situ method shows more optimal results and low solid-state reaction between the stainless-steel sheath and MgB_2 which impacts the formation of oxides. Choi et al., [3] carried out a carbon doping process on MgB_2 superconducting wire using the ex-situ powder in-tube method.

This study; put ready-made MgB_2 powder with > 99% purity into stainless steel (SS) metal tubes. This study used SS 304 steel tubes which were cheaper than other metal tubes. The

DOI : 10.55981/metalurgi.2023.694

Metalurgi is Sinta 2 Journal (https://sinta.kemdikbud.go.id/journals/profile/3708) accredited by Ministry of Education, Culture, Research, and Technology, Republic Indonesia

previous characterization also showed that the SS tube did not react with MgB_2 when heated [4]. Only a little research has been done to quantitatively characterize the crystallographic texture of MgB_2 superconducting wire, in addition to the frequency of publication topics that are not too high. The latest publication by Melone et al., [5] discusses the crystallographic texture of MgB_2 wire with SiC nano doping. Previously, Kováč et al., [6] discussed the anisotropy of the critical electric current (Ic) of in-situ MgB_2 in the form of bands, one of which is due to the texture of MgB_2 near the interface with the Fe, Ta, and Nb sheaths. Even further back, Song et al., [7] published articles on the anisotropy of grain morphology and crystallographic texture and their implications for the flux pinning mechanism of MgB_2 in the form of pellets, filaments, and thin films.

This research was conducted to characterize and analyze the crystallographic texture of MgB_2 in wire form, its hardness value, and microstructure morphology.

2. MATERIALS AND METHODS

MgB_2 powder with a purity > 99% was put into a SS 304 tube with an initial diameter of 6 mm. This MgB_2-containing SS 304 tube was rolled to reduce the wire diameter to 3.2 mm. Several tests were carried out on the rolled wire, including the Vickers hardness test, microstructure observation, XRD (x-ray diffraction) test, and crystallographic texture test.

In the Vickers hardness test, the cut and mounted wire samples were ground using abrasive paper numbers 40 to 2000 until the sample's surface was scratch-free. The samples were then polished using 1-micron alumina polishing fluid. The Vickers hardness test was performed using a pyramid-shaped diamond indenter. This test was carried out at five points with the same load, 0.3 N. The sample for the Vickers hardness test was also used for microstructure observation using a JEOL JSM-6390A SEM (scanning electron microscope).

For the XRD test, the wire sample was chopped or filed first to obtain a powder or flake form so that low-power x-rays can penetrate it. When a crystalline material is analyzed using XRD, the x-rays are diffracted at specific angles that depend on the spacing between the planes of atoms within the crystal lattice. Each set of planes diffracts the x-rays at a particular angle, producing a diffraction peak in the XRD pattern. The material's crystal structure can be determined by analyzing the positions and intensities of the diffraction peaks.

However, for x-rays to interact with the crystal lattice and produce diffraction peaks, the material must be powdered or flake. This is because x-rays have a limited penetration depth and are scattered in all directions when interacting with bulk material. By grinding or filing the sample into a powder or flake, the sample's surface area is significantly increased, allowing the x-rays to penetrate the material from many different directions and increasing the number of diffraction directions observed in the XRD pattern.

Increasing the number of diffraction directions is important because it provides more information about the material's crystal structure. The more diffraction directions observed, the more accurately the crystal structure can be determined, including the lattice parameters, space group, and the orientation of the crystal lattice concerning the sample surface. This information is important for understanding the material's physical properties, such as its mechanical, thermal, and electrical properties, and designing new materials with tailored properties.

XRD tests and analysis were carried out to determine the position of the Bragg peaks at a specific diffraction angle range and the percentage of elements contained in the MgB_2 superconducting wire, using the PANalytical EMPYREAN XRD test kit with Cu-Kα radiation, with a wavelength (λCu) of 1.54060 Å and a position angle between 10.0024° to 79.9684°.

Neutron diffraction is a powerful technique used to study the crystal structure of materials, particularly those that contain light elements such as hydrogen or lithium, which are difficult to analyze using x-ray diffraction. Neutron diffraction experiments are typically performed using a neutron source, such as a research reactor or a spallation source, which produces a beam of neutrons directed onto the sample.

The data from the XRD test with the PANalytical EMPYREAN instrument was then used to observe crystallographic textures with the neutron FCD/TD (four-circle diffractometer/texture diffractometer). The neutron FCD/TD (four-circle diffractometer/ texture diffractometer) is a specialized instrument used for neutron diffraction experiments. It consists of a sample stage that can rotate around four different axes, allowing the sample to be oriented in various positions concerning the neutron beam. The instrument is also equipped with detectors that can measure the intensity of the diffracted neutron beam at different angles,

which can be used to determine the crystal structure and orientation of the sample.

In a neutron diffraction experiment with the FCD/TD, the sample is first mounted onto the sample stage and oriented in a specific direction concerning the neutron beam. The neutron beam is then directed onto the sample, and the detectors detect the diffracted neutrons. By analyzing the positions and intensities of the diffracted neutron peaks, the material's crystal structure can be determined, including the positions of the atoms within the crystal lattice and the symmetry of the lattice.

In addition to determining the crystal structure, the FCD/TD can also be used to study crystallographic textures, which refer to the preferred orientation of the crystal lattice within the material. By rotating the sample stage around different axes and measuring the diffraction patterns at each orientation, it is possible to determine the preferred orientation of the crystal lattice and how it affects the material properties. This information is important for understanding the anisotropic properties of materials, such as their mechanical, thermal, and electrical properties, and for designing new materials with tailored properties.

This study used an FCD/TD (four-circle diffractometer/texture diffractometer) to determine the two-dimensional crystallographic texture of MgB_2 compounds with crystal orientation relative to the 2θ angles of the peak intensity of the XRD results. However, because FCD/TD used a neutron beam with a different wavelength (λn) than the Cu-Kα (λCu) wavelength from XRD PANalytical EMPYREAN, the 2θ angles of XRD had first to be converted to 2θ angles for FCD/ TD, using an equation based on Bragg's law:

$$\frac{\lambda_{Cu}}{\lambda_n} = \frac{\sin \theta_{Cu}}{\sin \theta_n} \quad (1)$$

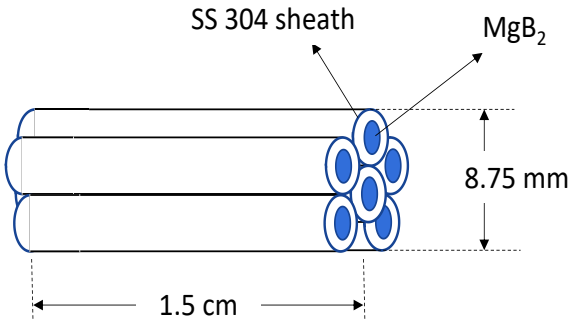

Figure 1. The bundle of MgB_2 wires

There were two types of wire samples for this neutron diffraction test, one with a diameter of 2.5 mm and the other with a diameter of 3 mm. The wire samples were bundled to provide a large enough surface area for diffraction. The average diameter of the bundled wires was 8.75 mm, with a length of 1.5 cm (Fig.1). The data resulting from neutron diffraction was then processed using the MAUD (materials analysis using diffraction) application.

3. Result and Discussion

3.1 Longitudinal Anatomy of Wire Samples

Figure 2 shows a sample of SS 304-sheathed MgB_2, which experienced a rolling reduction process. The diameter of the MgB_2 superconducting wire sample decreased from 6.0 mm to 3.2 mm, or a 71.6% reduction.

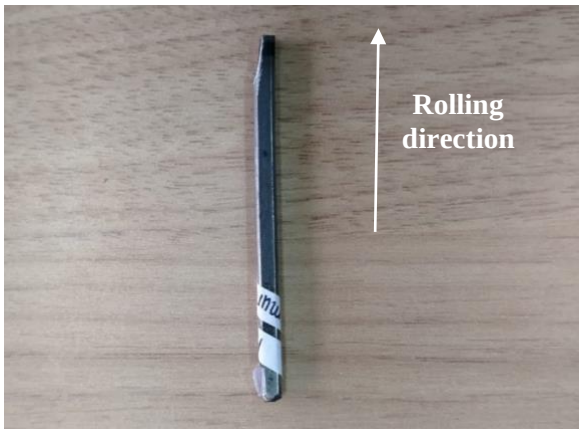

Figure 2. Sample of rolled MgB_2 superconducting wire

Figure 3 shows the longitudinal anatomy of this SS 304-sheathed MgB_2 wire sample, where the MgB_2 compound was flanked by SS 304. It can be seen that there was a longitudinal crack in the MgB_2 area due to the work-hardening phenomenon in the brittle MgB_2 solid.

Figure 4 shows the results of measuring the average thickness of the SS 304 tube and the MgB_2 area using the JEOL JSM-6390A SEM.

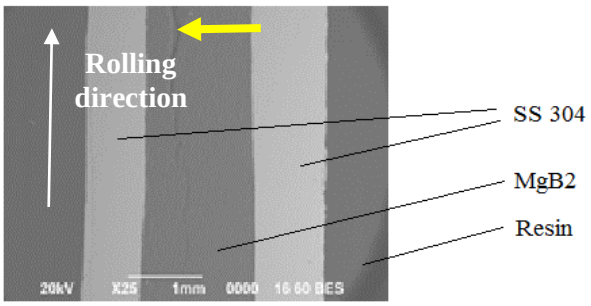

Figure 3. Longitudinal anatomy of a sample of rolled MgB_2 superconducting wire. The yellow arrow indicates the longitudinal crack in the MgB_2

Measurements of the diameter of the SS 304 wire sheath showed an average value of 3.224 mm and an inner diameter filled with MgB_2 of 1.428 mm.

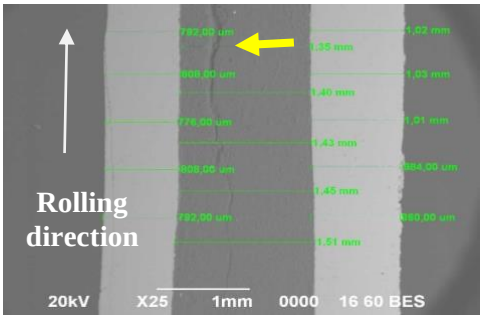

Figure 4. Measurement of the wire sample's average diameter, the thickness of the SS 304 tube, and the area of the MgB_2 compound. The yellow arrow indicates the longitudinal crack in the MgB_2

3.2 Hardness of Wire Samples

Table 1 shows the hardness value of each indentation and its average value.

Table 1. MgB_2 superconducting wire hardness values

Test No.	HV	Hardness (GPa)
1	357.8	3.5088
2	337.4	3.3087
3	317.6	3.1145
4	371.2	3.6402
5	391.5	3.8981

The Vickers hardness test took into account the value of diagonal 1 and diagonal 2 to obtain the HV hardness value using the following equation:

$$D = \frac{D1+D2}{2} \quad (2)$$

$$HV = \frac{2\,F\sin(136°/2)}{D} \quad (3)$$

$$HV = \frac{1{,}854\,F}{D^2} \quad (4)$$

where:
D = average diagonal length
D1 = length of diagonal 1
D2 = length of diagonal 2
HV = Vickers hardness value
F = load.

Based on Equations 2-4, the average hardness value of the MgB_2 superconducting wire was 355.1 HV (3.482 GPa). Previous research conducted by Herbirowo et al., [8] on SS 316-sheathed MgB_2 wire which was annealed at 800 °C and rolling, showed a hardness value of 377.2 HV. The difference in hardness values was mainly due to the nickel content in SS 304 and SS 316. SS 304 contains an average of 8.0% nickel, while SS 316 contains 10.0% nickel. The higher the nickel is, the value of the strength and hardness of the steel increases. In addition, SS 316 contains 2.0% Mo (molybdenum). Mo functions not only to increase corrosion resistance but also to increase steel's hardness, toughness, and strength.

3.3 Microstructures of MgB_2 Wire

Figure 5 shows the morphology of the MgB_2 compound on a superconducting wire. Clumping or agglomeration (white arrows) occurred in the MgB_2 compound due to the rolling process, where the MgB_2 powder wire was subjected to roll compaction pressure. The inhomogeneity of agglomerate sizes in MgB_2 powder was determined by several factors, such as the outer and inner diameters of the wire, the rolling or rolling tool system, and the interaction between process parameters and the physical properties of the material (MgB_2 and SS 304 sheath) [9].

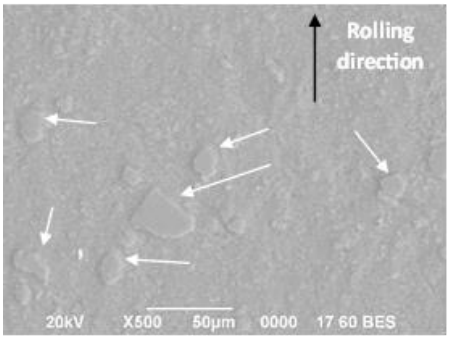

Figure 5. Morphology of MgB_2 compounds in superconducting wire samples. Agglomerations with non-uniform size distribution are indicated by white arrows

EDS analysis of these lumps also indicated the presence of the second phase (Mg)B-O (discussed later). At the same spot as Fig. 5, an elemental mapping analysis was carried out to determine the distribution of the main elements, as shown in Fig. 6.

From Figure 6, it can be seen that the most dominant elements were Mg (Fig. 6(d)), then O (Fig. 6(c)), and B (Fig. 6(b)). The presence of elemental oxygen indicated the occurrence of an oxide phase. Figure 7 shows the results of the analysis of the EDS *in-situ* composition by spot on several lumps or agglomerates. These lumps were suspected to be the second phase (Mg)B-O with various compositions (Figs. 7(a)-(c), and (e)).

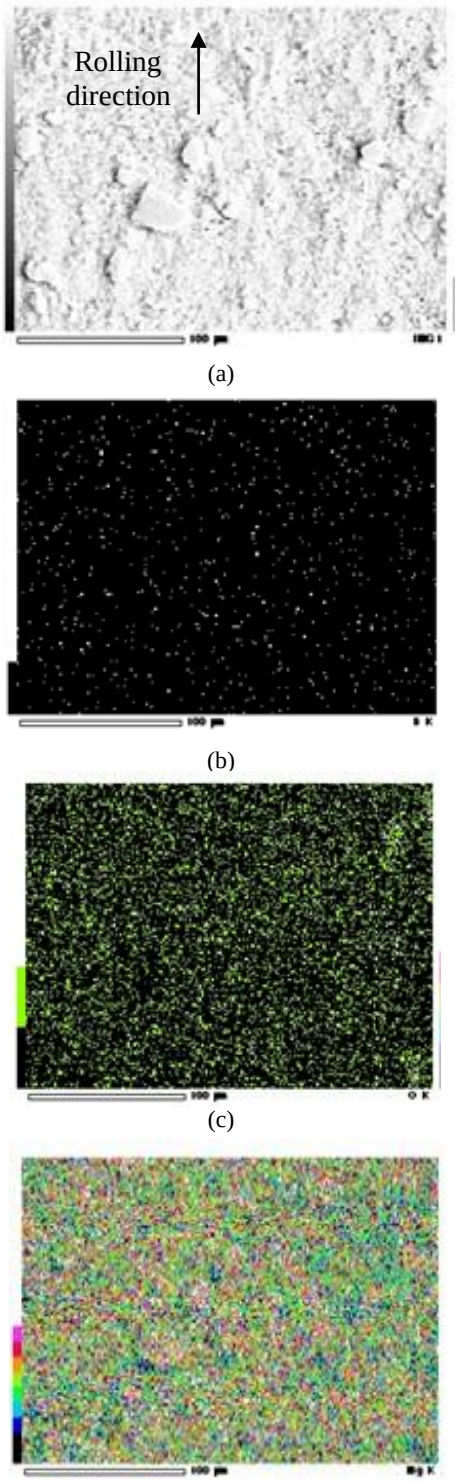

Figure 6. Results of elemental mapping analysis on MgB_2 superconducting wire samples: (a) SEM, (b) elemental boron (B) (c) elemental oxygen (O), and (d) elemental magnesium (Mg)

The existence of the second phase (Mg)B-O was also previously reported by Chen et al., [10], where the element oxygen originated from the boron powder precursor, B_2O_3.

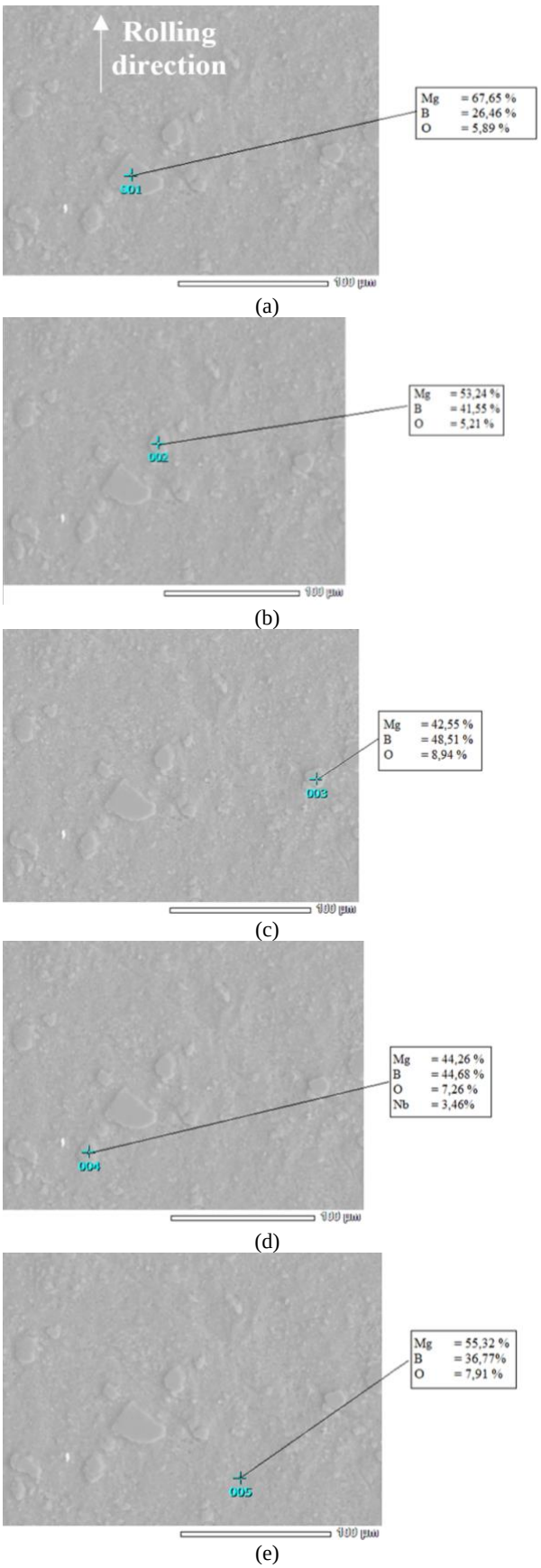

Figure 7. The EDS in-situ composition analysis results by spot on the agglomerates of the MgB_2 compound indicated the presence of a second phase (Mg)BO with various composition variations

Amorphous boron contains more B_2O_3 compounds than crystalline boron. However, after synthesis, the second phase (Mg)B-O is mainly produced by crystalline boron [10]. The results of the EDS analysis of the agglomerates in Fig. 7(d) show the presence of Nb (niobium) impurity.

3.4 X-Ray Diffraction Analysis

Figure 8 shows the XRD results of the MgB_2 superconducting wire sample, where the highest peak of the MgB_2 compound occurs at an angle of $2\theta = 42.428°$ and for iron (Fe) from the SS 304 sheath at 44.510°. The compositional analysis of the XRD results showed an MgB_2 content of 74.1% and α iron of 25.9%.

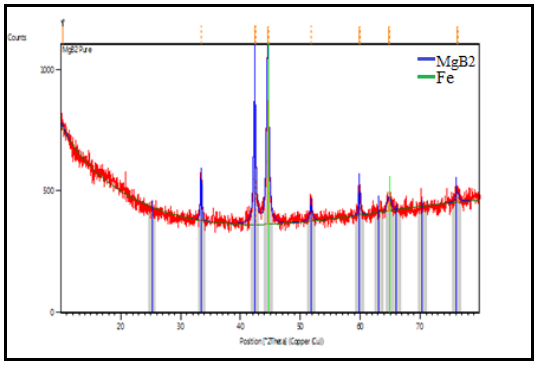

Figure 8. Graph of XRD characterization results of MgB_2 superconducting wire

3.5 Crystallography Analysis

Previously it was known that the maximum intensity of MgB_2 occurred at an angle of $2\theta_{Cu} = 42.428°$ or $\theta_{Cu} = 21.214°$. By using the values of $\lambda_{Cu} = 1.54060$ Å and $\lambda_n = 1.2799$ Å and Equation 1, the value of the angle θ_n was calculated to be 17.495°, or $2\theta_n = 34.989°$. The results of the diffraction data from FCD/TD were then processed in the MAUD (material analysis using diffraction) application.

Two types of phases were observed using FCD/TD, namely γ-Fe (austenite) and MgB_2. Austenitic steel hasana fcc (face-centered cubic) structure with a space group of Fm-3m. Depending on the carbon content, the lattice parameter of γ-Fe varies from 3.5680 Å (C = 0.45%) to 3.6043 Å (C = 1.25%) [11]. MgB_2 has a hexagonal structure with lattice parameters a = b = 3.06 Å c= 3.52 Å, $\alpha = 90°$, $\beta = 90°$, $\gamma = 120,°$ and a space group of P6/mmm [12]-[13].

From the results of the initial analysis of the Bragg peak with MAUD, there was good compatibility between the Bragg peaks of the austenitic γ-Fe phase with the experimental results, as shown in Fig. 9 (for wire diameter = 3.0 mm) and Fig. 10 (for wire diameter = 2.5 mm).

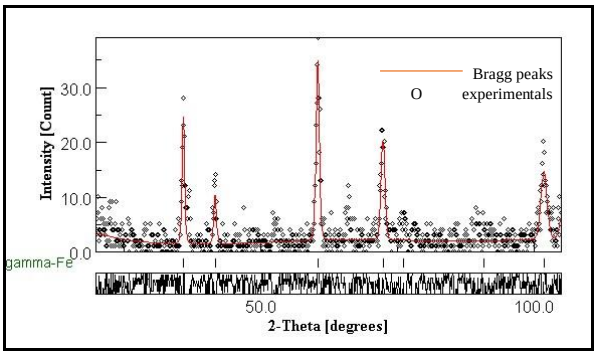

Figure 9. The compatibility between γ-Fe phase Bragg peaks with the experimental results, for wire diameter = 3.0 mm

The difference in peak intensities in Fig. 9 and Fig. 10 can be correlated with the extent of wire reduction. The wire reduction was 75.0% for a wire diameter of 3.0 mm, whereas the wire reduction was 82.6% for a wire diameter of 2.5 mm. Such wire reduction induced the development of crystallographic texture or preferred orientations due to material deformation [13]-[14].

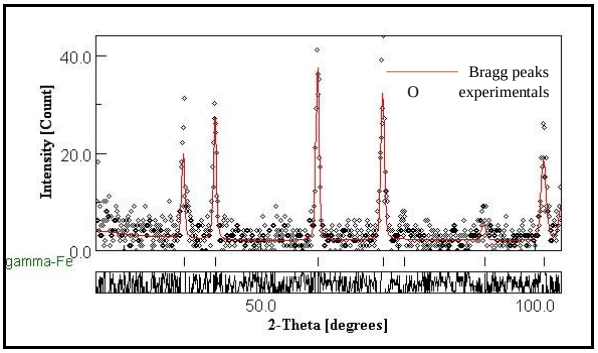

Figure 10. The compatibility between γ-Fe phase Bragg peaks with the experimental results, for wire diameter = 2.5 mm

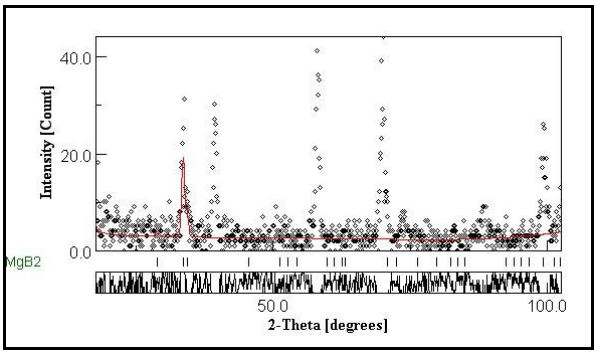

Figure 11. No compatibility between MgB_2 Bragg peaks with the experimental results, for wire diameter = 3.0 mm

In the MgB_2 phase, there was no Bragg peak corresponding to the theoretically produced MgB_2 Miller index for both wires with diameters

of 2.5 mm and 3.0 mm (Figs. 11 and 12). There is no Bragg peak in the MgB_2 diffraction pattern since boron, and its boride compound are neutron-absorbing materials [15]-[16]. Even though the abundance of ^{10}B isotope in nature is only 18.9-20.4% [17], it has a neutron cross-section of 3835-3840 barns (1 barn = $10^{-24}cm^2$) for 0.025 eV neutron [18]. On the other hand, the ^{11}B isotope (with the 79.6-81.1% portion) has a neutron cross-section of only 5.28 barns [18]-[19].

To overcome this issue, researchers may use other techniques such as neutron diffraction, which is more sensitive to the presence of ^{10}B, or use isotopically enriched samples containing a higher proportion of ^{11}B. These methods can help to improve the resolution and accuracy of the XRD analysis of MgB_2.

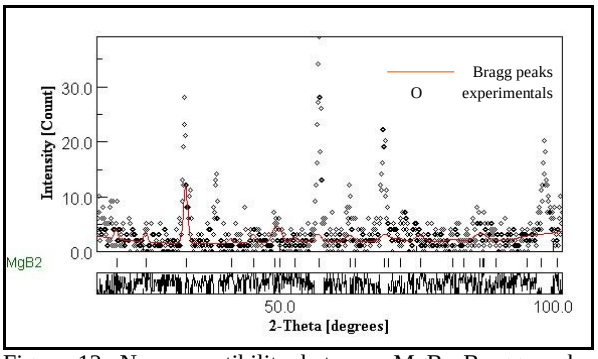

Figure 12. No compatibility between MgB_2 Bragg peaks with the experimental results, for wire diameter = 2.5 mm

4. CONCLUSION

The average hardness value of the MgB_2-SS 304 superconducting wire was 355.1 HV (3.482 GPa), lower than that of the MgB_2-SS 316 superconducting wire. This condition was triggered by the higher Ni and Mo content in SS 316 compared to SS 304. Observation of the microstructure of the MgB_2 compound on this superconducting wire shows the presence of agglomerates of various sizes, which were also the second (Mg)B-O phase with variations in composition. There were no obvious Bragg peaks in the MgB_2 phase. This was probably due to the effect of the very large neutron absorption cross-section of the ^{10}B isotope so that most of the neutrons were absorbed by the material, and only a small part of neutrons was scattered and captured by the detector. The detected Bragg peaks came from the austenitic (γ-Fe) of SS 304-sheath.

ACKNOWLEDGMENT

The authors would like to thank and appreciate the neutron scattering laboratory of the Research Center for Radiation Detection and Nuclear Analysis Technology and the ferrous materials research group of the Research Center for Metallurgy, National Research and Innovation Agency of Indonesia for their scientific and technical supports so that samples and neutron-diffraction data can be obtained.

REFERENCES

[1] N. Nurmalita, N. Amani, and F. Fauzi, "XRD analysis of Bi-2212 superconductors prepared by the self-flux method," *Jurnal Natural*, vol. 13, no. 1, pp. 23-27, 2013. Doi:10.24815/jn.v13i1.841

[2] Y. P. Sun, W. H. Song, J. M. Dai, B. Zhao, J. J. Du, H. H. Wen, and Z. X. Zhao, "Superconductivity at 49 K in copper doping magnesium diboride," *arXiv preprint cond-mat/0103101*, 2001.

[3] S. Choi, D. Patel, J. H. Kim, H. Kumakura, A. Matsumoto, G. Nishijima, S. H. Kim, J. Joo, and M. Maeda, "Evaluation and control of residual amorphous phases in carbon-doped MgB_2 superconductors," *J. Alloys Compd.*, vol. 864, pp. 158867, 2021. Doi:10.1016/j.jallcom.2021.158867.

[4] S. Herbirowo, M. N. Hanafi, A. Imaduddin, E. P. Utomo, Hendrik, A. Trenggono, and E. Yustanti, "Pengaruh doping nikel dan suhu sinter pada pembuatan kawat superkonduktor magnesium diborida," *Indonesian Journal of Applied Physics*, vol. 10, no. 2, pp. 116-125, 2020.

[5] M. Melone, M. Moran, F. Malamud, M. T. Malachevsky, and A. Serquis, "Crystallographic texture study of nano-SiC-doped MgB_2 wires," *IEEE Transactions on Applied Superconductivity*, vol. 31, no. 5, pp. 1-5, 2021. Doi: 10.1109/TASC.2021.3068088.

[6] P. Kováč, T. Melišek, and I. Hušek, "Ic anisotropy of in situ made MgB_2 tapes," *Supercond Sci Technol*, vol. 18, no. 7, pp. L45-L48, 2005. Doi:10.1088/0953-2048/18/7/L02.

[7] X. Song, S. E. Babcock, C. B. Eom, D. C. Larbalestier, K. A. Regan, R. J. Cava, S. L. Bud'Ko, P. C. Canfield, and D. K. Finnemore, "Anisotropic grain morphology, crystallographic texture and their implications for flux pinning mechanisms in MgB_2 pellets, filaments, and thin films," *Supercond Sci Technol*, vol. 15, no. 4, pp. 511-518, 2002. Doi: 10.1088/0953-2048/15/4/306.

[8] S. Herbirowo, V. Puspasari, H. Nugraha, E. Sulistiyo, A. W. Pramono, and A. Imaduddin, "Fabrikasi kawat resistansi nol

berbahan MgB2/stainless steel dengan variasi reduksi ukuran melalui pengerolan dingin terhadap karakteristik mekanik dan struktur mikro," *Energi & Kelistrikan*, vol. 13, no. 2, pp. 242-249, 2021. Doi: 10.33322/energi.v13i2.1491.

[9] L. P. Gandarillas, A. P. Gago, A. Mazor, P. Kleinebudde, O. Lecoq, and A. Michrafy, "Effect of roll-compaction and milling conditions on granules and tablet properties," *European Journal of Pharmaceutics and Biopharmaceutics*, vol. 106, pp. 38-49, 2016. Doi: 10.1016/j.ejpb.2016.05.020.

[10] S. K. Chen, K. A. Yates, M. G. Blamire, and J. L. M. Driscoll, "Strong influence of boron precursor powder on the critical current density of MgB_2," *Supercond Sci Technol*, vol. 18, no. 11, pp. 1473-1477, 2005. Doi:10.1088/0953-2048/18/11/011.

[11] J. Mazur, "Lattice parameters of martensite and austenite," *Nature*, vol. 166, no. 4228, pp. 828-828, 1950. Doi: 10.1038/166828a0.

[12] A. Jain, S. P. Ong, G. Hautier, W. Chen, W. D. Richards, S. Dacek, S. Cholia, D. Gunter, D. Skinner, G. Ceder, and K. A. Persson, "Commentary: The materials project: a materials genome approach to accelerating materials innovation," *APL Mater*, vol. 1, no. 1, pp. 011002, 2013. Doi: 10.1063/1.4812323.

[13] S. T. Faris, "Analysis of plane strain rolling rigid plastic materials using finite element method," *Diyala Journal of Engineering Sciences*, vol. 8, no. 2, pp. 99-115, 2015. Doi:10.24237/djes.2015.08208.

[14] A. Pramono and J. Bouffette, *Pengantar tekstur kristalografi: teori dan aplikasi*. LIPI Press, 2022. Doi:10.14203/press.393.

[15] I. Hore-Lacy, "Nuclear Power," *Nuclear Energy in the 21st Century*, pp. 37-53, 2007. Doi:10.1016/B978-012373622-2/50006-4.

[16] "Neutron Absorber - an overview | ScienceDirect Topics." https://www.sciencedirect.com/topics/earth-and-planetary-sciences/neutron-absorber (accessed Jan. 03, 2023).

[17] S. Barth, "Boron isotopic analysis of natural fresh and saline waters by negative thermal ionization mass spectrometry," *Chem Geol*, vol. 143, no. 3-4, pp. 255-261, 1997. Doi:10.1016/S0009-2541(97)00107-1.

[18] N. Soppera, M. Bossant, O. Cabellos, E. Dupont, and C. J. Díez, "Janis: NEA java-based nuclear data information system," *EPJ Web Conf*, vol. 146, pp. 07006, 2017. Doi:10.1051/epjconf/201714607006.

[19] E. C. Auden, H. M. Quinn, S. A. Wender, J. M. O'Donnell, P. W. Lisowski, J. S. George, N. Xu, D. A. Black, and J. D. Black, "Thermal neutron-induced single-event upsets in microcontrollers containing boron-10," *IEEE Trans Nucl Sci*, vol. 67, no. 1, pp. 29-37, 2020. Doi: 10.1109/TNS.2019.2951996.